GSK3β mediates muscle pathology in myotonic dystrophy

Karlie Jones,[1] Christina Wei,[1] Polina Iakova,[2] Enrico Bugiardini,[3] Christiane Schneider-Gold,[4] Giovanni Meola,[3] James Woodgett,[5] James Killian,[6] Nikolai A. Timchenko,[2] and Lubov T. Timchenko[1]

[1]Department of Molecular Physiology and Biophysics and [2]Department of Pathology and Immunology and Huffington Center on Aging, Baylor College of Medicine, Houston, Texas, USA. [3]Department of Neurology, University of Milan, IRCCS Policlinico San Donato, Milan, Italy. [4]Department of Neurology, St. Josef Hospital of the Ruhr-University of Bochum, Bochum, Germany. [5]Samuel Lunenfeld Research Institute, Mount Sinai Hospital, Toronto, Ontario, Canada. [6]Department of Neurology, Baylor College of Medicine, Houston, Texas, USA.

Myotonic dystrophy type 1 (DM1) is a complex neuromuscular disease characterized by skeletal muscle wasting, weakness, and myotonia. DM1 is caused by the accumulation of CUG repeats, which alter the biological activities of RNA-binding proteins, including CUG-binding protein 1 (CUGBP1). CUGBP1 is an important skeletal muscle translational regulator that is activated by cyclin D3–dependent kinase 4 (CDK4). Here we show that mutant CUG repeats suppress Cdk4 signaling by increasing the stability and activity of glycogen synthase kinase 3β (GSK3β). Using a mouse model of DM1 (*HSA^{LR}*), we found that CUG repeats in the 3′ untranslated region (UTR) of human skeletal actin increase active GSK3β in skeletal muscle of mice, prior to the development of skeletal muscle weakness. Inhibition of GSK3β in both DM1 cell culture and mouse models corrected cyclin D3 levels and reduced muscle weakness and myotonia in DM1 mice. Our data predict that compounds normalizing GSK3β activity might be beneficial for improvement of muscle function in patients with DM1.

Introduction

Myotonic dystrophy type 1 (DM1) is a complex disease affecting primarily skeletal muscle, causing myotonia, skeletal muscle weakness, and wasting (1). DM1 is caused by the expansion of polymorphic, noncoding CTG repeats in the 3′ untranslated region (UTR) of the dystrophia myotonica protein kinase (*DMPK*) gene (2, 3). The severity of DM1 correlates with the length of CTG expansions. The longest CTG expansions are observed in patients with a congenital form of DM1 that affects newborn children (1). Congenital DM1 is characterized by a delay in skeletal muscle development, leading to extreme muscle weakness and a weak respiratory system, which has been associated with a high mortality rate (4, 5). Expanded CTG repeats cause the disease through RNA CUG repeats that misregulate several CUG RNA-binding proteins, including CUGBP1 (CUGBP Elav-like family member 1, CELF1) and muscleblind 1 (MBNL1) (6–24). The mutant CUG aggregates sequester MBNL1, reducing splicing of MBNL1-regulated mRNAs (11, 12, 17). A portion of the mutant CUG repeats bind to CUGBP1 and elevate CUGBP1 protein levels through an increase in its stability (14). Phosphorylation of CUGBP1 by PKC also contributes to the increase in CUGBP1 stability (24).

CUGBP1 is a highly conserved, multifunctional protein that regulates RNA processing on several levels, including translation, RNA stability, and splicing (9, 14–16, 18, 20–22, 25–32). The increase in CUGBP1 to the levels observed in the congenital DM1 leads to the delay of myogenesis in the CUGBP1 transgenic mouse model (18). Multiple functions of CUGBP1 are tightly regulated by phosphorylation at distinct sites (21, 22, 24). Phosphorylation of CUGBP1 by AKT at S28 controls nucleus-cytoplasm distribution of CUGBP1 and increases CUGBP1 affinity toward certain mRNA targets (21, 22). Translational activity of CUGBP1 is regulated by cyclin D3/CDK4 phosphorylation at S302 (21, 22, 29, 32). p-S302–CUGBP1 binds to the active eukaryotic initiation translation factor 2α (eIF2α) (22, 29, 32). The CUGBP1-eIF2 complex delivers mRNAs to polysomes and promotes their translation (29). Since CUGBP1 regulates translation of proteins crucial for skeletal muscle development (such as a cyclin-dependent kinase inhibitor, p21, cyclin D1, and myocyte enhancer factor 2A), the translational function of CUGBP1 is important for normal myogenesis, especially at the stage of formation of multinucleated myotubes (15, 18, 21). In DM1 myotubes, CUGBP1 does not bind to active eIF2 because CUGBP1 is under-phosphorylated at S302. This reduction of phosphorylation of CUGBP1 is associated with the reduction of cyclin D3 levels in DM1 myotubes (21). As a result, the fusion of DM1 myotubes occurs with low efficiency, delaying myogenesis. Correction of cyclin D3 levels in DM1 myoblasts improves formation of multinucleated myotubes (21). Based on these data, we hypothesized that the normalization of cyclin D3 in DM1 might be beneficial for DM1 patients and might correct DM1 skeletal muscle pathology.

In the current study, we tested this hypothesis by investigating upstream events that cause the reduction of cyclin D3 in DM1. We found that the reduction of cyclin D3 in DM1 muscle biopsy samples is associated with the phosphorylation of cyclin D3 at T283 by active GSK3β kinase. Our data show that correction of the GSK3β/cyclin D3 pathway in the DM1 mouse model (*HSA^{LR}* mice) improves skeletal muscle strength and reduces myotonia.

Results

Increase in GSK3β in muscle biopsy samples from patients with DM1. Our previous study has shown that cyclin D3 is reduced in the cytoplasm of DM1 cultured myotubes (21). To determine whether cyclin D3 is also reduced in mature muscle in DM1, we initially examined cyclin D3 levels in muscle biopsies from 2 sex- and age-matched normal controls and from 2 patients with DM1. This analysis showed that the protein levels of cyclin D3 are reduced in DM1 skeletal muscle (Figure 1A).

Conflict of interest: The authors have declared that no conflict of interest exists.

Citation for this article: *J Clin Invest.* 2012;122(12):4461–4472. doi:10.1172/JCI64081.

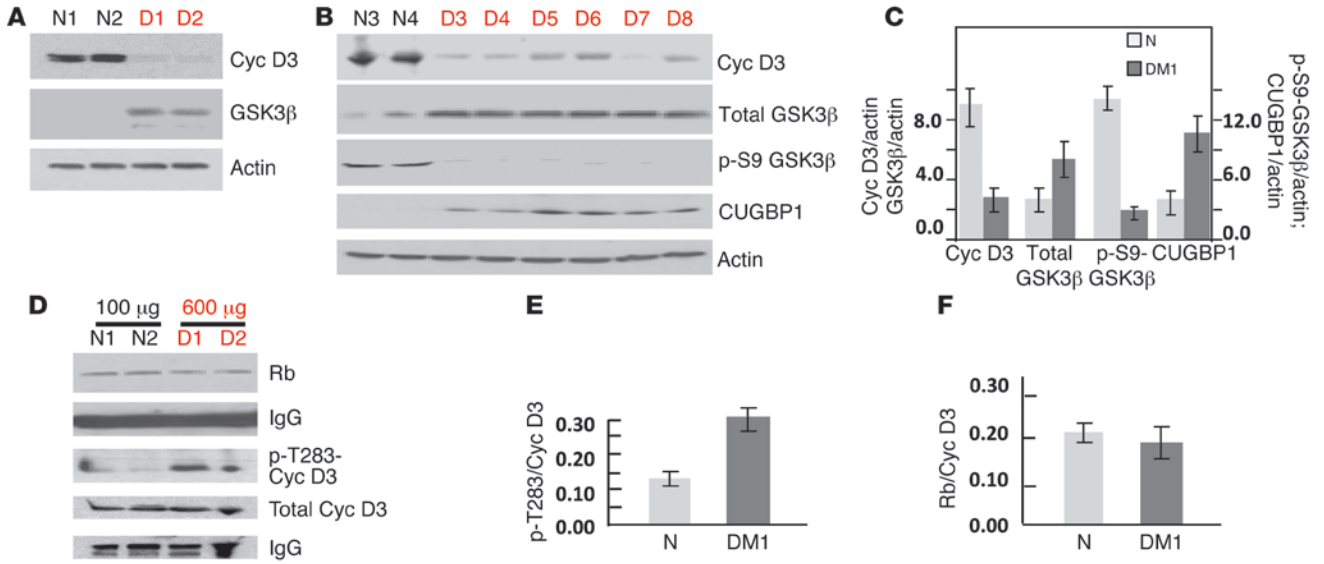

Figure 1

Elevation of active GSK3β and reduction of cyclin D3 in DM1 skeletal muscle biopsies. (**A**) Western blot analyses of the total protein extracts from patients with normal muscle histopathology (N1, N2) and from patients affected with DM1 (D1, D2) were performed, with antibodies shown on the right. (**B**) Examination of GSK3β/cyclin D3/CUGBP1 pathway in skeletal muscles of 6 additional patients with DM1. Western blotting was performed with antibodies to cyclin D3 (Cyc D3), GSK3β, p-S9–GSK3β, CUGBP1, and actin. (**C**) Average levels of cyclin D3, GSK3β, p-S9–GSK3β, and CUGBP1 presented as ratios to actin. The standard deviations represent quantitation of protein expression based on 3 experiments. (**D**) Phosphorylation of cyclin D3 at T283 is increased in DM1 skeletal muscle biopsies. IP–Western blot assay. Cyclin D3 was precipitated with antibodies to total cyclin D3. Cyclin D3 IPs were divided into two portions and examined by Western blot assay with antibodies to Rb, p-T286 (recognizing p-T283 in cyclin D3), and total cyclin D3. The signal of IgGs is the control for antibodies used for immunoprecipitation. Since cyclin D3 is reduced in DM1, the amount of protein from DM1 muscle tissue used for IP was 6-fold higher than that isolated from normal muscle. Ratios of p-T283–cyclin D3 (**E**) and Rb (**F**) to total cyclin D3 were determined by quantitating protein expression from **D**. The standard deviations show values based on 3 experiments.

It is known that cyclin D3 is mainly regulated at the level of protein stability by two mechanisms (33, 34). The first mechanism of cyclin D3 regulation involves GSK3β-mediated phosphorylation of cyclin D3 at T283, which triggers degradation of cyclin D3 through the ubiquitin/proteasome pathway (33). The second mechanism is mediated by the interaction of cyclin D3 with phospho–retinoblastoma protein (p-Rb). This interaction protects cyclin D3 from degradation (34). To examine whether GSK3β is involved in the downregulation of cyclin D3 in DM1, we measured the total levels of GSK3β in the muscle biopsy samples from DM1 patients. Western blot analysis showed that the levels of total GSK3β increased in the DM1 muscle samples (Figure 1A).

To confirm the reduction of cyclin D3 in DM1, we performed immunoanalysis of 6 additional muscle biopsy samples from the patients with DM1 and from 2 additional samples from patients with normal muscle histopathology. Cyclin D3 levels were reduced in all 8 examined patients with DM1 (Figure 1, A–C). Western blot analysis also showed that levels of total GSK3β were increased in all studied DM1 muscle biopsy samples (Figure 1, A–C).

GSK3β is a constitutively active protein kinase, the activity of which is inhibited by phosphorylation of S9 by other upstream kinases (35). We measured the levels of p-S9–GSK3β in the muscle biopsy samples from normal patients and patients with DM1 and found that the inactive form (phosphorylated at S9) of GSK3β was almost undetectable in DM1 muscle (Figure 1, B and C). Such reduction in the inactive p-S9–GSK3β and increase in total GSK3β in DM1 muscle shows that active GSK3β is elevated in DM1.

One of the well-characterized markers of DM1 molecular pathology is the increase in CUGBP1 (14, 16, 19, 23). We found that the same muscle extracts from patients with DM1 showed elevation of CUGBP1 relative to normal muscle samples (Figure 1, B and C).

To further examine the mechanism of the reduction in cyclin D3 in DM1, we asked whether the increase in GSK3β in DM1 skeletal muscle might lead to the increased phosphorylation of cyclin D3 at T283 (p-T283–cyclin D3). In these experiments, we also examined the second mechanism of cyclin D3 regulation, which is mediated by the interaction of cyclin D3 with p-Rb. Cyclin D3 was precipitated from normal and from DM1 muscle samples using antibodies to total cyclin D3. The cyclin D3 IPs were divided into two portions; one portion was examined by Western blotting with antibodies to p-Rb, and the other was probed with antibodies against p-T286–cyclin D1. The antibodies against p-T286 of cyclin D1 recognize both p-T286 and p-T283 in cyclins D1 and D3, respectively (36). We found that the phosphorylation of cyclin D3 at T283 was increased in DM1 muscle biopsy samples, whereas interaction of cyclin D3 with Rb was not changed in DM1 samples (Figure 1, D–F). Note that to pull down identical amounts of cyclin D3, we used 6-fold-greater amounts of the proteins from DM1 muscle biopsy than those from normal muscle biopsy samples. Under these conditions, the total levels of cyclin D3 in the IPs from normal and DM1 samples were identical; however, the levels of p-T283–cyclin D3 increased almost 3-fold in DM1 samples. Thus, we suggest that cyclin D3 is reduced in DM1 due to increased phosphorylation at T283 by GSK3β, which triggers the degradation of cyclin D3 (33).

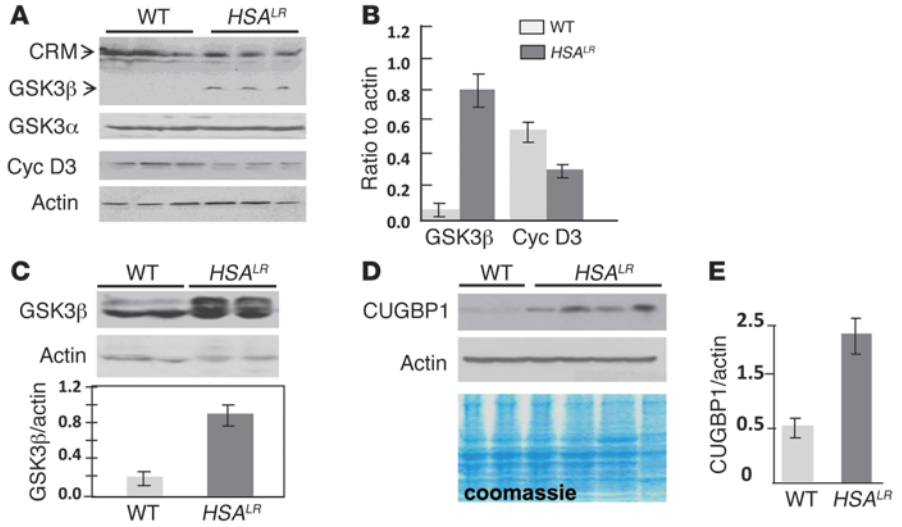

Figure 2

The expansion of CUG repeats increases GSK3β protein in skeletal muscle from *HSA^{LR}* mice. (**A**) Levels of total GSK3α, GSK3β, cyclin D3, and actin were determined by Western blot analyses of total protein extracts from skeletal muscle (soleus) of *HSA^{LR}* mice (at 6 months of age) and extracts from matching WT mice. CRM, cross-reactive material. (**B**) Ratios of signals of GSK3β and cyclin D3, as presented in **A**, to actin. The standard deviations for 3 experiments are shown. (**C**) GSK3β is increased in skeletal muscle of 1-month-old *HSA^{LR}* mice. Protein extracts from skeletal muscle (gastroc) of 1-month-old WT and *HSA^{LR}* mice were analyzed by Western blot with antibodies to total GSK3β and re-probed with antibodies to actin. Shown are ratios of GSK3β signals, as presented in **C**, to actin. The standard deviations shown are based on 3 repeats. (**D**) CUGBP1 is increased in muscle of *HSA^{LR}* mice. Protein extracts from skeletal muscle (soleus) of age-matched *HSA^{LR}* and WT mice were analyzed by Western blot assay. The membrane was re-probed with antibodies to actin and stained with Coomassie blue to verify protein loading and integrity. (**E**) Ratios of CUGBP1 signals presented in **D** (as an average of 4 mutant and 2 WT mice) to actin signals. The standard deviations are shown for 3 experiments.

Mutant CUG repeats increase expression of GSK3β in a mouse model of DM1. To determine whether the mutant CUG repeats may be responsible for elevation of GSK3β and downregulation of cyclin D3, we examined levels of GSK3β and cyclin D3 in muscle of a mouse model of DM1, *HSA^{LR}* mice (11). These mice express an array of the untranslated CUG repeats in the 3′ UTR of human skeletal actin (11). We found that levels of total GSK3β were elevated in skeletal muscle (soleus) from *HSA^{LR}* mice; whereas cyclin D3 was reduced in the same protein extracts (Figure 2, A and B). The elevation of GSK3β in the muscle of *HSA^{LR}* mice was detected in adult (6-month-old) (Figure 2, A and B) and in young (1-month-old) mice (Figure 2C). In skeletal muscle of young *HSA^{LR}* mice, GSK3β migrated as a double band that may represent differentially phosphorylated GSK3β (Figure 2C). Since many functions of GSK3α and -β are similar, we analyzed the levels of GSK3α in skeletal muscle of these mice and found no significant changes for this enzyme (Figure 2A). Analysis of CUGBP1 levels showed that, similar to that in DM1 muscle, CUGBP1 levels were increased in skeletal muscle of *HSA^{LR}* mice (Figure 2, D and E). Taken together, these data show that the mutant CUG repeats increase levels of GSK3β and reduce cyclin D3.

Misregulation of GSK3β in DM1 myogenesis. Our previous studies with the DM1 human muscle cell model showed that cyclin D3 is increased in normal myogenesis at the stage of formation of multinucleated myotubes (21). We have also shown that cyclin D3 activates phosphorylation of CUGBP1 at S302 and that the amounts of active CUGBP1-eIF2 complexes are increased during normal myotube differentiation (21). In contrast to normal myogenesis, DM1 myotubes have reduced levels of cytoplasmic cyclin D3 (21). Since GSK3β is elevated in DM1 myofibers and because GSK3β regulates cyclin D3, we thought that GSK3β might be misregulated in DM1 myogenesis. To examine this suggestion, we have compared the levels of total GSK3β in the course of normal and DM1 myogeneses using human muscle cell models. As seen in Figure 3, A, C, and D, protein levels of GSK3β are reduced during normal differentiation in both cytoplasm and nuclei of myotubes. However, in cytoplasm of DM1 myotubes, the expression of GSK3β is increased compared with that in normal myogenesis (Figure 3, A–C). In normal nuclei, GSK3β levels are reduced during differentiation; however, in DM1 nuclei the levels of GSK3β remain high in myoblasts and in myotubes (Figure 3, A, B, and D). In agreement with data showing that active GSK3β reduces cyclin D3, the cells with increased levels of GSK3β had reduced levels of cyclin D3 (Figure 3, A, B, E, and F). These data show that DM1 muscle cell precursors have lost proper regulation of nucleus-cytoplasm distribution of GSK3β during myogenesis and that this aberrant expression of GSK3β is involved in a failure of DM1 myoblasts to increase cyclin D3.

GSK3β is increased in DM1 muscle cell precursors due to protein stabilization. Data in Figure 1, B and C, show that the levels of inactive p-S9–GSK3β were reduced in DM1 muscle biopsies. Since the active form of GSK3β is phosphorylated at Y216 (37), we examined the levels of p-Y216–GSK3β in DM1 muscle samples. As shown in Figure 4A, p-Y216–GSK3β is increased in DM1 muscle biopsies. Consistent with this finding, inactive p-S9–GSK3β was reduced in DM1, whereas total GSK3β was increased.

It has been shown that autophosphorylation of GSK3β at Y216 increases stability of GSK3β (37). To determine whether the elevation of GSK3β in DM1 occurs due to increased stability of GSK3β, we treated normal and DM1 myoblasts with cyclohexamide (CHX) to block new protein synthesis and measured levels of total GSK3β at different time points after CHX addition. We found that the half-life of GSK3β was very short in normal myoblasts. The levels of GSK3β were sharply reduced in 1 hour after CHX addition and remained at low levels during the whole course of the treatment with CHX (Figure 4, B and C). However, in DM1 myoblasts, levels of GSK3β were essentially unchanged 1 hour after treatment with CHX (Figure 4, B and C). Although GSK3β levels were reduced after 2 and 4 hours of CHX addition to DM1 myoblasts, levels remained higher than those in normal myoblasts. Thus, stability of GSK3β protein is increased in DM1.

To determine whether the inhibition of the CUG-elevated GSK3β normalizes cyclin D3 levels, we utilized recently generated monoclonal CHO cell lines with Tet-regulated transcription of the

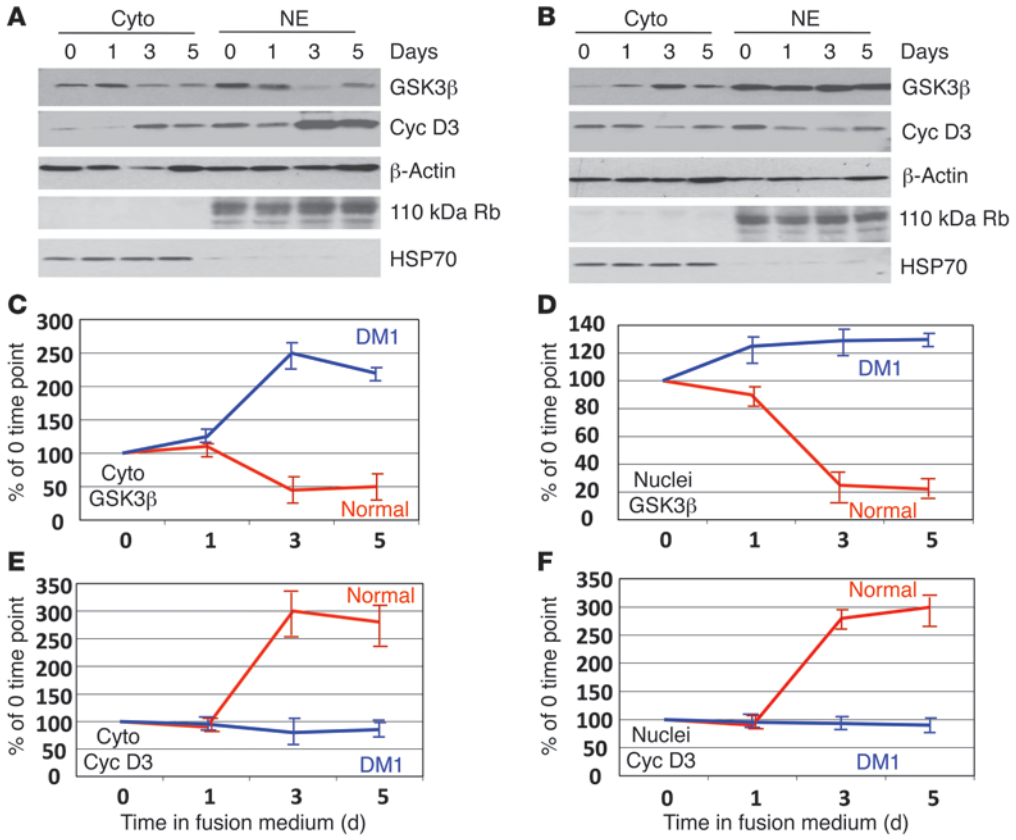

Figure 3

Misregulation of GSK3β expression in DM1 myogenesis. Western blot analysis of cytoplasmic (Cyto) and nuclear proteins from normal (**A**) and DM1 myoblasts (**B**) at different stages of differentiation (1, 3, and 5 days in the fusion medium) with antibodies to total GSK3β, total cyclin D3, and β-actin as control. To verify the separation of nuclear and cytoplasmic proteins, the protein extracts were probed with antibodies to a nuclear protein, Rb, and to a preferentially cytoplasmic protein, HSP70. Curves show the quantification of GSK3β (**C** and **D**) and cyclin D3 (**E** and **F**) signals (adjusted to β-actin) as percentage of signals for these proteins at each time point relative to 0 time point in cytoplasm (**C** and **E**) and in nuclei (**D** and **F**) of normal and DM1 myoblasts. Intensities of GSK3β and cyclin D3 signal in myoblasts (0 time point of differentiation) were counted as 100%. The *x* axis shows number of days in the differentiation medium. The standard deviations represent values for 3 experiments.

mutant CUG repeats (CUG_{914}) (22, 38). In this DM1 cell model, the transcription of the mutant CUG repeats is induced with a single addition of doxycycline (Dox), allowing the early detection of the mutant CUG repeats by Northern blot and FISH assays at 7 hours after Dox addition (refs. 22, 38, and Supplemental Figure 1; supplemental material available online with this article; doi:10.1172/JCI64081DS1). It has been previously shown that the mutant CUG repeats are almost undetectable at 3 and 6 hours after Dox addition, because only a small percentage of cells (2%–4%) showed CUG repeat aggregates at these time points (38). However, at 7 hours after Dox addition, the mutant CUG repeats are detectable by FISH hybridization (Supplemental Figure 1 and ref. 38). CUG_{914} RNA was degraded 48 hours after Dox addition (Supplemental Figure 1 and refs. 22, 38). Immunoanalysis of GSK3β in this cell model showed that the mutant CUG repeats increase total levels of GSK3β at 7 hours after Dox addition (Figure 5, A and B). GSK3β levels continued to increase at 17 hours after Dox addition and then were reduced at 24 and 48 hours. We examined whether GSK3β is elevated during the period 1–7 hours after Dox addition and detected the increase of GSK3β as early as 2 hours after Dox addition (Figure 5, C and D). These results show that elevation of GSK3β occurs at an early stage of the expression of CUG repeats before the buildup of CUG aggregates. The kinetics of GSK3β elevation mimicked early accumulation and partial degradation of the mutant CUG repeats (Figure 5A, Supplemental Figure 1, and refs. 22, 38). Examination of the levels of the p-Y216 form of GSK3β after induction of transcription of the mutant CUG repeats showed that the increase in the levels of p-Y216–GSK3β mimicked the kinetics of the elevation of total GSK3β (Figure 5A). Thus, the mutant CUG repeats increase GSK3β stability through the increase in autophosphorylation of GSK3β. In agreement with the elevation of GSK3β, cyclin D3 levels were reduced after CUG_{914} transcription was initiated. The reduction in cyclin D3 at 7 hours after Dox addition was significantly weaker (1.2-fold) than the increase in GSK3β (5-fold), suggesting that the reduction in cyclin D3 follows the increase of GSK3β. In agreement with this suggestion, an 8-fold increase in GSK3β at 17 hours after Dox addition led to a 2.5-fold reduction in cyclin D3 (Figure 5, A and B).

To examine whether inhibition of GSK3β could correct cyclin D3 levels, monoclonal CHO cells expressing the mutant CUG repeats after Dox addition were treated with lithium, a known inhibitor of GSK3 (35). This treatment partially corrected the total levels of GSK3β (Figure 5, E and F). Partial reduction of

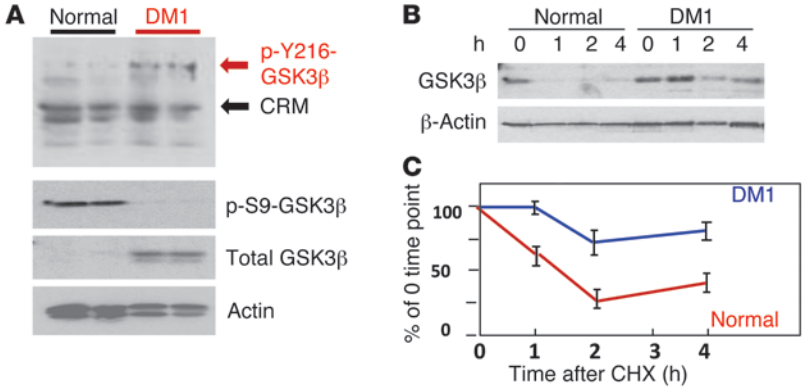

Figure 4

GSK3β is increased in DM1 due to stabilization of the protein. (**A**) p-Y216–GSK3β is increased in DM1 muscle biopsies. Western blot analysis of total protein extracts from 2 normal and 2 DM1 patients with antibodies to active p-Y216–GSK3β, inactive p-S9–GSK3β, total GSK3β, and actin is shown. Antibodies to p-Y216–GSK3β cross-react with other proteins (CRM). (**B**) GSK3β stability is increased in DM1 muscle cell precursors. Protein synthesis was inhibited by CHX; and GSK3β levels were measured by Western blot analysis in normal and in DM1 myoblasts at different time points (1, 2, and 4 hours) after CHX addition. β-Actin shows the loading of proteins. (**C**) Quantification of GSK3β stability in normal and DM1 myoblasts. The *y* axis shows GSK3β signals (as ratios to β-actin) in cells treated with CHX as percentages of GSK3β signal in the untreated cells. The signal of GSK3β in the untreated cells was counted as 100%. The *x* axis shows the time of treatment with CHX (in hours). The standard deviations represent values of 3 experiments.

GSK3β protein levels suggests that the inhibition of autophosphorylation of GSK3β might reduce stability of GSK3β and thus normalize its levels. To test this possibility, we measured the levels of p-Y216–GSK3β in CUG-expressing cells treated with lithium and found that the activated p-Y216 form of GSK3β was not detectable in the treated cells (Figure 5E). Thus, inhibition of GSK3β activity by lithium inhibits the autophosphorylation of GSK3β at Y216 and reduces stability of GSK3β. Normalization of GSK3β levels and activity in the CUG-expressing cells treated with lithium corrected levels of cyclin D3 with respect to controls (Figure 5, E and F).

The expanded CUG repeats cause skeletal muscle weakness in the HSA^{LR} mouse model. The above results suggest that the mutant CUG repeats misregulate the GSK3β/cyclin D3 pathway. As previously shown, the reduction in cyclin D3 leads to a reduction in CUGBP1 phosphorylation at S302, and this event inhibits CUGBP1 translational activity in DM1 muscle cells (21, 22). Such inhibition of CUGBP1 could reduce translation of some mRNAs essential for muscle function, leading to the skeletal muscle wasting and weakness. In agreement with this prediction, our recent analysis of muscle structure and function in a mouse model with disrupted CUGBP1 and in mice in which S302 is replaced with alanine shows that myogenesis and muscle strength are severely affected in these mice (C. Wei and L. Timchenko, unpublished observations). Since the GSK3β/cyclin D3 pathway is altered in muscle of *HSA^{LR}* mice, we tested whether *HSA^{LR}* mice develop muscle weakness. Grip strength has been analyzed in *HSA^{LR}* mice of different ages (1, 3, and 6 months). We found that at 1 month of age, the grip strength of *HSA^{LR}* mice was slightly reduced or unchanged relatively to that in the 1-month-old WT mice. However, at 3 and at 6 months of age, the muscle strength in *HSA^{LR}* mice was reduced by 17%–21% compared with that in WT mice of the same age (Figure 6A). It is important to note that *HSA^{LR}* mice show variability in muscle weakness even within the same line. We found that in the line 20LRb, the majority of *HSA^{LR}* mice developed muscle weakness, whereas approximately 20% of mice showed the same grip strength as age- and sex-matched WT mice. Such variability of phenotype in the mouse model of DM1 correlates with a strong variability of DM1 severity, ranging from asymptomatic to lethal (1). The phenotype variability in DM1 is associated with meiotic instability of CTG repeat expansions, with an increase in the length of CTG repeats from generation to generation (1). DM1 is also characterized by somatic instability of CTG repeat expansions, with changes in the length of CTG repeats in different tissues of patients with DM1 and with an increase in the length of CTG repeats with age (1). Recent studies predict that the length of CTG expansions might change in patients with DM1 at different rates (39). Thus, it is predicted that the length of CTG repeats might increase in *HSA^{LR}* mice in the succeeding generations due to meiotic instability. It is also possible that other factors (genetic modifiers) might have different effect on the instability of the mutant CUG repeats in different littermates.

We next asked whether the reduction in grip strength in *HSA^{LR}* mice was due to a myofiber loss. Total myofibers were counted on maximal transverse sections of gastrocnemius (gastroc) and tibialis anterior (TA) muscles from 6-month-old *HSA^{LR}* and WT mice. We found that the number of myofibers was reduced by 27% in TA ($P < 0.05$) and by 44% in gastroc ($P < 0.0005$) in the 6-month-old *HSA^{LR}* mice (Figure 6B). The total number of myofibers was also reduced in other muscle groups in *HSA^{LR}* mice of this age (data not shown). The reduction in myofiber number in skeletal muscle of the 6-month-old *HSA^{LR}* mice was accompanied by an increase in the average myofiber area of approximately 27% in TA ($P < 0.0005$) and by 46% in gastroc ($P < 0.0005$) relative to WT mice of the same age (Figure 6C), probably due to compensatory response to the loss of myofiber number.

In contrast to the 6-month-old *HSA^{LR}* mice, the total number of myofibers in the 1-month-old *HSA^{LR}* mice increased by 32% in gastroc and by 28% in TA (Figure 6B). However, myofibers in the 1-month-old *HSA^{LR}* mice were smaller in size relative to those in the 1-month-old WT mice (Figure 6C). The average myofiber area was reduced in TA of 1-month-old *HSA^{LR}* mice by 13% and in gastroc by 20% in comparison to age-matched WT controls (Figure 6C). We suggest that the increase in myofiber number in 1-month-old *HSA^{LR}* mice is mediated by the activation of muscle regeneration in response to the accumulation of CUG repeats that initiate muscle damage. This idea is consistent with a significant increase in nuclei located beneath the basal lamina surrounding myofibers in the 1-month-old *HSA^{LR}* mice (Figure 6D), which likely represent satellite cells activated in response to myofiber damage caused by CUG expansions. The number of these nuclei increased by 44% in the TA of 1-month-old *HSA^{LR}* mice and by 31% in gastroc relative to that in the 1-month-old WT mice. In contrast, the number of nuclei beneath the basal lamina

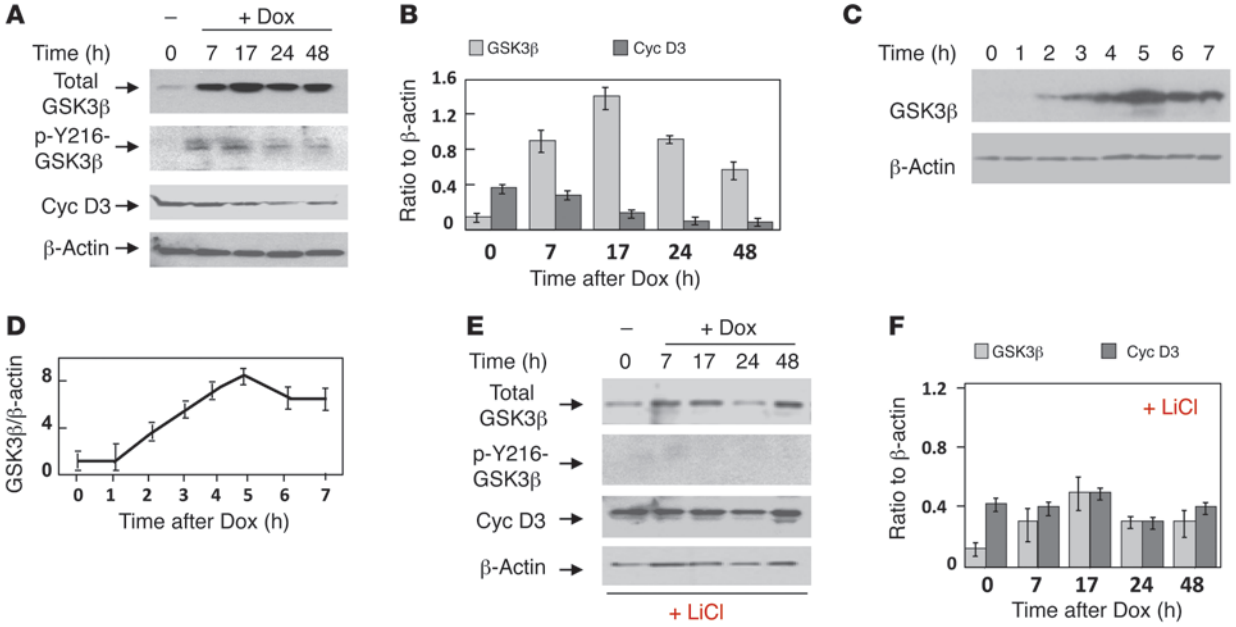

Figure 5

Inhibition of GSK3β activity corrects cyclin D3 levels in CUG-expressing CHO cells. (**A**) Accumulation of mutant CUG repeats elevates active GSK3β and reduces cyclin D3. Western blot analysis of cytoplasmic protein extracts from CHO double-stable CUG-expressing monoclonal cells before addition of Dox (time 0) and at different time points after Dox addition (shown on the top) with antibodies to total GSK3β, p-Y216–GSK3β, total cyclin D3, and β-actin. (**B**) Ratios of GSK3β and cyclin D3 signals to β-actin (*y* axis), based on protein expression in **A**. The standard deviations represent values of 3 experiments. The *x* axis shows time after Dox addition (in hours). (**C**) GSK3β is increased at early time points after Dox treatment. Proteins were isolated in 1–7 hours after Dox addition and analyzed by Western blotting with antibodies to total GSK3β and β-actin. (**D**) The ratios of GSK3β signals to β-actin signals of protein expression shown in **C** are presented in the *y* axis. The *x* axis shows time points after Dox addition. The standard deviations show values of 3 experiments. (**E**) Lithium normalizes cyclin D3 levels in CUG-expressing CHO cells. Western blot analysis of the protein extracts isolated as described in **A**, but cells after Dox addition were treated with 20 μM LiCl for 7 hours. (**F**) Ratios of GSK3β and cyclin D3 signals observed in **E** to β-actin (*y* axis). The *x* axis shows time after Dox addition (in hours). Standard deviations based on 3 repeats are shown.

was reduced by 13% in TA of the 6-month-old HSA^{LR} mice and by 32% in gastroc ($P < 0.05$) (Figure 6D).

The alterations in the number of nuclei beneath the basal lamina prompted us to compare the number of activated satellite cells in young and adult HSA^{LR} muscle to that in age- and sex-matched WT mice. We examined the paired box protein Pax-7 as a marker of newly activated satellite cells. To compare the number of activated proliferating satellite cells, we extracted myogenic cells from the whole gastroc of matching mice, plated them on cell culture slides, and subjected them to immunofluorescence analysis with antibodies to Pax-7. We found that the number of activated Pax-7–positive cells extracted from gastroc of young (2 months old) HSA^{LR} mice was 2.3-fold greater than that in gastroc of the matching WT mice ($P < 0.0004$) (Figure 6E and Supplemental Figure 2). In contrast to young mice, the number of newly activated proliferating satellite cells was around 1.7 times lower in gastroc of 7-month-old HSA^{LR} mice than in matching WT mice ($P < 0.036$) (Figure 6E and Supplemental Figure 3).

We compared Pax-7 expression in muscle extracts from young (1-month-old) and adult (6-month-old) WT and HSA^{LR} mice. As shown in Figure 6F, the levels of Pax-7 were increased in young HSA^{LR} muscle, but they were reduced in the muscle from adult HSA^{LR} mice. These results suggest that the activation of satellite cells in the 6-month-old HSA^{LR} mice is probably diminished, leading to reduced fiber regeneration, a reduction in total fiber number, and skeletal muscle weakness. This is in contrast to the young HSA^{LR} mice, in which Pax-7 was elevated and muscle weakness was not detected.

One of the outcomes of CUG toxicity in muscle is the accumulation of internal myonuclei. H&E staining showed small numbers of internal nuclei in 1-month-old muscle of HSA^{LR} mice: an average of 1.4 nuclei per field in TA and 0.8 nuclei per field in gastroc (Figure 6G). However, at 6 months of age, there was a significant increase in internal nuclei in muscle of HSA^{LR} mice: 6.6 nuclei per field in TA ($P < 0.05$) and 11 nuclei per field in gastroc ($P < 0.005$). Taken together, these results show that adult HSA^{LR} mice develop muscle weakness accompanied by a reduction in activated satellite cells, an increase in internal nuclei, suggesting repetitive cycles of degeneration and regeneration, and a reduction in myofiber number.

Treatments of HSA^{LR} mice with lithium and TDZD-8 correct the GSK3β/cyclin D3 pathway in skeletal muscle. To examine whether the inhibition of GSK3β could correct cyclin D3, we treated HSA^{LR} mice with lithium and found that levels of GSK3β were reduced in skeletal muscle (gastroc) of HSA^{LR} mice after treatment (Figure 7A). The levels of cyclin D3 were also normalized. Since lithium also acts as a Mg^{2+} competitive inhibitor and may have other targets, we used an additional inhibitor of GSK3β, 4-benzyl-2-methyl-1,2,4-thiadiazolidine-3,5-dione (TDZD-8). Similar to the treatment with lithium, the treatment of HSA^{LR} mice with TDZD-8

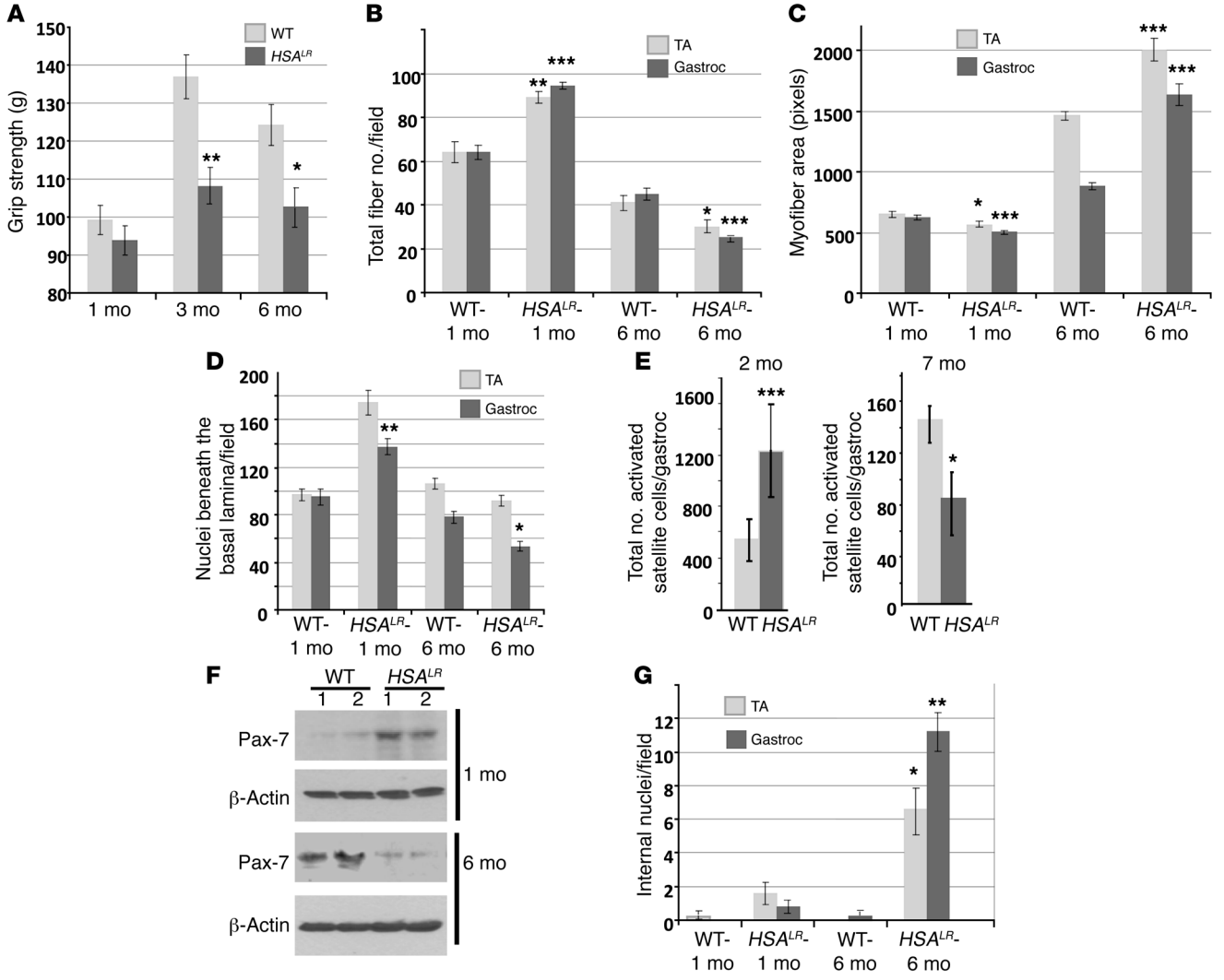

Figure 6

Muscle weakness in adult *HSA*^{LR} mice is accompanied by a reduction of activated myogenic satellite cells. (**A**) A reduction of muscle strength in *HSA*^{LR} mice. Grip strength in WT and *HSA*^{LR} mice of different ages (1, 3, and 6 months). **P* < 0.05, ***P* < 0.005. (**B**) Increase in myofiber number in young (1 month old) and reduction of myofiber number in adult (6 months old) *HSA*^{LR} mice. Total number of fibers per field (×20) in maximal cross section areas of TA and gastroc from matched WT and *HSA*^{LR} mice. **P* < 0.05, ***P* < 0.005, ****P* < 0.0005. (**C**) Myofiber area is reduced in young (1 month old) *HSA*^{LR} mice but increased in adult (6 months old) *HSA*^{LR} mice. The *y* axis shows average fiber area (in pixels). **P* < 0.05, ****P* < 0.0005. (**D**) The number of nuclei beneath the basal lamina varies in young and adult *HSA*^{LR} mice. The *y* axis shows the number of nuclei beneath the basal lamina in TA and gastroc from young and adult *HSA*^{LR} mice per field (×20). **P* < 0.05, ***P* < 0.005. (**E**) The number of activated Pax-7–positive cells is increased in young (2 months old) but reduced in adult (7 months old) *HSA*^{LR} mice. The *y* axis shows total number of activated Pax-7–positive cells isolated from whole gastroc of matched WT and *HSA*^{LR} mice. **P* < 0.036, ****P* < 0.0004. (**F**) Levels of Pax-7 protein are increased in 1-month-old and reduced in adult *HSA*^{LR} mice. Muscle samples from soleus of age- and sex-matched WT and *HSA*^{LR} mice were examined by Western blot assay with antibodies to Pax-7 and β-actin, as a control for protein loading. (**G**) Increase in internal nuclei in myofibers of *HSA*^{LR} mice. The average number of internal nuclei per field (×20) in 1-month- and 6-month-old WT and *HSA*^{LR} mice, based on the analyses of 200–300 fibers, is shown. **P* < 0.05, ***P* < 0.005. SEM is shown.

normalized the levels of GSK3β in *HSA*^{LR} muscle and corrected the expression of cyclin D3 (Figure 7B).

Correction of the GSK3β/cyclin D3 pathway in muscles of *HSA*^{LR} mice treated with lithium also restored CUGBP1 translational function. CUGBP1 forms a complex with inactive p-S51–eIF2 in skeletal muscle of *HSA*^{LR} mice (Figure 7C). It has been previously shown that this complex is a repressor of translation (22). After the animals were exposed to a lithium-containing diet, the amounts of complexes containing CUGBP1 and inactive p-S51–eIF2 were significantly reduced. This result shows that the improvement of GSK3β/cyclin D3 in skeletal muscle of *HSA*^{LR} mice reversed inhibition of CUGBP1 translational activity caused by the mutant CUG repeats.

Lithium and TDZD-8 treatments improve skeletal muscle strength and reduce myotonia in skeletal muscle of HSA^{LR} *mice*. To examine whether the correction of the GSK3β/cyclin D3/CUGBP1 pathway improved muscle strength, we measured grip strength before and after the treatment of *HSA*^{LR} mice with lithium. We found that a

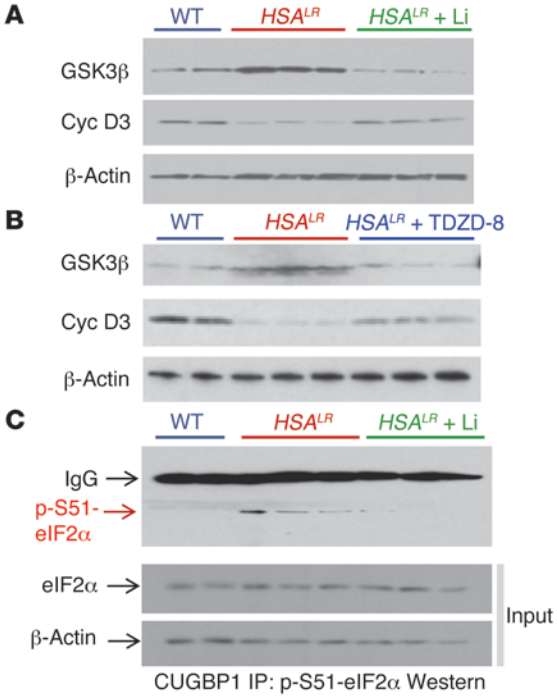

Figure 7
Inhibition of GSK3β corrects levels of cyclin D3 and translational activity of CUGBP1 in skeletal muscle of *HSA*^{LR} mice. Western blot analysis of GSK3β and cyclin D3 in skeletal muscle (gastroc) of 6-month-old WT and *HSA*^{LR} mice before and after treatment with lithium (**A**) and TDZD-8 (**B**). β-Actin shows protein loading. (**C**) Lithium reduces amounts of the translation repressor complexes CUGBP1–p-S51–eIF2α in skeletal muscle of *HSA*^{LR} mice. Top panel: CUGBP1 was precipitated with anti-CUGBP1 from skeletal muscle of 6-month-old WT and *HSA*^{LR} mice, treated and untreated with lithium, and the IPs were probed with antibodies to p-S51–eIF2α. Heavy chain IgGs signals are also shown. Bottom panels (input): Western blotting with antibodies to the total eIF2α. The membrane was reprobed with β-actin.

2-week lithium-containing diet improved skeletal muscle strength in *HSA*^{LR} mice from 73% to 93% ($P < 0.0001$) of the WT mouse strength measurements (Figure 8A). Lithium improved muscle strength in *HSA*^{LR} mice of both 3 and 6 months of age.

We next examined whether lithium improves muscle histopathology in *HSA*^{LR} mice. H&E staining showed that lithium treatment reduced the number of internal nuclei in TA of treated *HSA*^{LR} mice from 7.6 nuclei to 4.4 nuclei per field ($P < 0.01172$) (Figure 8, B and C). However, in gastroc, the number of internal nuclei was almost unchanged (data not shown).

Since accumulation of CUG repeats in *HSA*^{LR} mice also causes myotonia, we examined whether lithium treatment has any effect on myotonia. Like that of muscle weakness, the severity of myotonia is variable in the 20LRb line of *HSA*^{LR} mice. We found that lithium treatment reduced myotonia in the treated animals (Table 1). A positive effect of lithium on myotonia was observed in *HSA*^{LR} mice of different ages, including 3-month- and 6-month-old mice. Switching to the regular diet after 2 weeks of lithium-containing chow reversed muscle weakness in *HSA*^{LR} mice; however, the beneficial effect of the lithium on myotonia remained during 4 weeks after lithium withdrawal (data not shown). This finding suggests that even small treatment terms of lithium are beneficial for reduction of myotonia in *HSA*^{LR} mice.

To confirm that the beneficial effect of lithium on muscle pathology in *HSA*^{LR} mice is mediated by inhibition of GSK3β, we examined the effect of TDZD-8 on the muscle strength of *HSA*^{LR} mice. We found that the treatment of *HSA*^{LR} mice with TDZD-8 improved the grip strength by 20.1% ($P < 0.009880$) (Figure 9A).

Improvement of muscle strength in *HSA*^{LR} mice treated with lithium and TDZD-8 suggests that the correction of GSK3β might have a positive effect on myofiber regeneration. Since levels of the marker of satellite cells Pax-7 are reduced in adult *HSA*^{LR} mice (Figure 6F), we examined whether TDZD-8 treatment improves Pax-7 expression in *HSA*^{LR} muscle. Western blot analysis showed that TDZD-8 normalized the levels of Pax-7 in gastroc from *HSA*^{LR} mice (Figure 9B).

Correction of Pax-7 levels in the *HSA*^{LR} mice treated with TDZD-8 suggested that activation of satellite cells in the treated mice might be improved. We compared the number of activated Pax-7 satel-

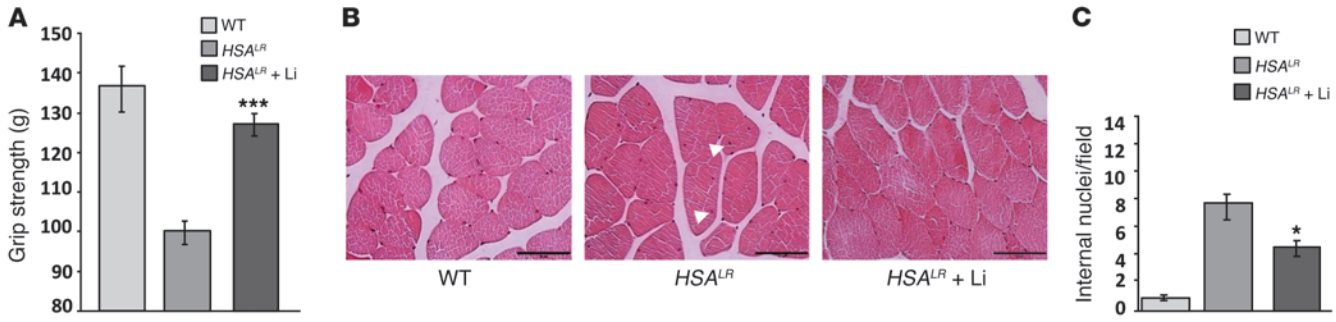

Figure 8
Lithium reduces skeletal muscle weakness in *HSA*^{LR} mice. (**A**) Improvement of grip strength in the *HSA*^{LR} mice treated with lithium. Grip strength in 3-month-old *HSA*^{LR} mice before and after treatment with lithium is shown. ***$P < 0.0001$ (treated *HSA*^{LR} mice vs. untreated *HSA*^{LR} mice). SEM is shown. (**B**) H&E staining. Representative images of transverse cross-sections stained with H&E from TA of 6-month-old WT and *HSA*^{LR} mice before and after treatment with lithium. Arrowheads indicate internal nuclei in TA of *HSA*^{LR} mice before treatment with lithium. Scale bars: 75 μm. (**C**) Lithium reduces the number of internal nuclei in TA muscle from *HSA*^{LR} mice. The *y* axis shows the number of internal nuclei, determined by H&E staining, based on analysis of 200–300 fibers in a maximal region of the transverse sections of TA of 6-month-old *HSA*^{LR} mice before and after treatment with lithium. As a normal control, internal nuclei were counted in 200–300 fibers in matching muscle of 6-month-old WT mice. *$P < 0.01172$ (treated *HSA*^{LR} mice vs. untreated *HSA*^{LR} mice). SEM is shown.

Table 1
Lithium reduces myotonia in 3-month-old *HSA^{LR}* mice

Mouse no.	Myotonia before Li+	Myotonia after Li+	Change in myotonia
1	+++ (5)	++ (5)	↓
2	+++ (5)	+ (3) and ++ (2)	↓
3	+++ (5)	+ (3) and ++ (2)	↓
4	++ (2) and +++ (3)	+ (3) and ++ (2)	↓
5	++ (5)	+ (1) and 0 (4)	↓
6	+++ (5)	0 (1) and + (4)	↓

Myotonic runs were measured 5 times in each *HSA^{LR}* mouse, and the severity of myotonia is expressed from + to +++, where + corresponds to weak myotonia and +++ corresponds to severe myotonia. The values in parentheses show the number of measurements of myotonia with the same severity.

lite cells in gastroc from *HSA^{LR}* mice treated and untreated with TDZD-8 and found that the number of newly activated Pax-7–positive cells increased in the treated mice by 40.9% ($P < 0.02952$) (Figure 9C). As a result, the number of activated Pax-7 cells was 10.9% greater in *HSA^{LR}* treated mice than that in the matched WT mice. Thus, correction of the GSK3β/cyclin D3/CUGBP1 pathway in *HSA^{LR}* mice has a positive effect on the activation of satellite cells, improving muscle strength.

Similar to lithium treatment, the treatment of *HSA^{LR}* mice with TDZD-8 reduced myotonia (Table 2). These data show that the correction of GSK3β improves muscle strength and reduces myotonia in *HSA^{LR}* mice.

Discussion

Despite numerous investigations into DM1 pathology, the detailed mechanism underlying this multisystem disease is not well understood, and therapeutic approaches have remained underdeveloped. In this study, we found that the active GSK3β is elevated in skeletal muscle biopsy samples from DM1 patients (Figure 1). The increase in GSK3β in DM1 occurs due to accumulation of mutant CUG repeats. This conclusion was made based on studies of two DM1 models: *HSA^{LR}* mice, expressing CUG repeats in the 3′ UTR of skeletal muscle actin; and CHO double-stable clones expressing Tet-regulated pure CUG repeats. In agreement with our findings, a recent study has shown disruption of AKT/GSK3β signaling in neuronal cells in response to the expression of CUG repeats (40).

Our data from the monoclonal CHO cell lines indicate that the elevation of GSK3β is an early event caused by the accumulation of small amounts of mutant CUG repeats. The mutant CUG repeats in this cell model are detectable by FISH and Northern blot assays mainly at 7 hours after Dox addition (Supplemental Figure 1 and ref. 38). We found that GSK3β increased within 2 hours after induction of CUG_{914} expression, suggesting that even small amounts of CUG repeats, which are difficult to detect by FISH assay, are sufficient to elevate GSK3β. The mechanism of CUG repeat–dependent elevation of active GSK3β involves the stabilization of GSK3β through an increase in its activity. This conclusion is supported by results indicating that inhibition of GSK3β activity by lithium corrected GSK3β protein levels (Figure 5E). Since the stabilization of GSK3β correlates with an increase in its autophosphorylation, the most likely mechanism is that CUG repeats first increase activity of GSK3β, and this in turn activates GSK3β phosphorylation, stabilizing GSK3β. How might CUG repeats activate GSK3β? Since RNA-binding activity of GSK3β has not been reported, it is clear that there is a pathway mediator that is activated by CUG repeats. Protein factors or toxic peptides, synthesized from expanded CUG RNA through an AUG-independent mechanism, might trigger the elevation of GSK3β activity (41). These factors involved in activating a CUG-mediated increase in GSK3β remain to be identified.

One of the most important results of this study is the identification of GSK3β as a crucial signaling molecule associated with the reduction of cyclin D3 and muscle weakness and myotonia in *HSA^{LR}* mice. Whereas initial reports had not described progressive muscle weakness and wasting in these mice, we found reproducible and statistically significant reduction of muscle strength in 3-month- and 6-month-old *HSA^{LR}* mice. Our data

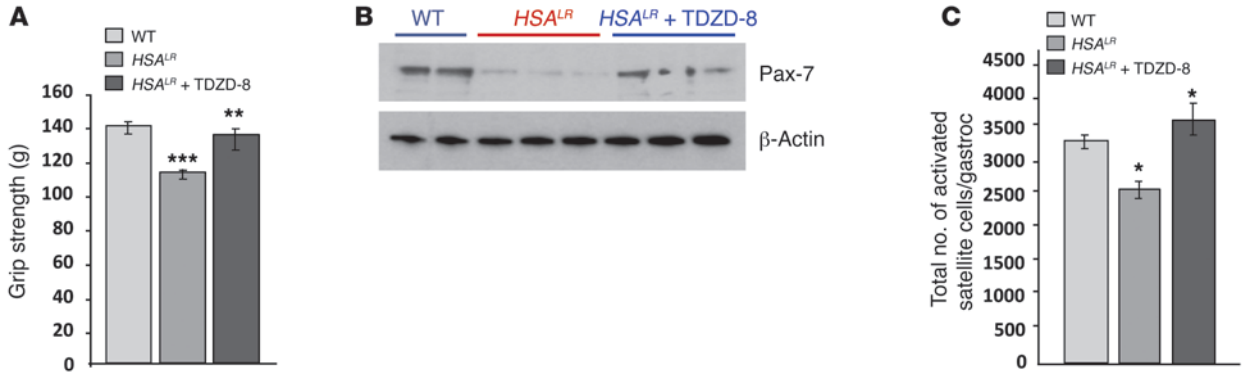

Figure 9
TDZD-8 treatment improves skeletal muscle strength in *HSA^{LR}* mice. (**A**) Improvement of grip strength in *HSA^{LR}* mice treated with TDZD-8. Grip strength in the 3-month-old *HSA^{LR}* mice before and after treatment with TDZD-8. SEM is shown. $^{**}P < 0.009880$, $^{***}P < 0.00006$. (**B**) Treatment of *HSA^{LR}* mice with TDZD-8 normalizes levels of Pax-7. Western blot analysis of protein extracts from matching muscles (gastroc) from 3-month-old WT mice, untreated *HSA^{LR}* mice, and *HSA^{LR}* mice treated with TDZD-8 was performed with antibodies to Pax-7. β-Actin shows protein loading. (**C**) TDZD-8 treatment increases the number of activated Pax-7–positive cells. The *y* axis shows total number of Pax-7–positive cells isolated from gastroc of 4-month-old WT and *HSA^{LR}* mice, untreated ($^{*}P < 0.010838$, untreated *HSA^{LR}* mice vs. matching WT mice) and treated with TDZD-8 ($^{*}P < 0.02952$, treated *HSA^{LR}* mice vs. untreated *HSA^{LR}* mice) (see Methods).

Table 2
TDZD-8 reduces myotonia in 3-month-old *HSA^{LR}* mice

Mouse no.	Myotonia before TDZD-8	Myotonia after TDZD-8	Change in myotonia
1	+++ (5)	+ (3) and ++ (2)	↓
2	+++ (5)	+ (4) and ++ (1)	↓
3	+++ (4) and 0 (1)	++ (5)	↓
4	+++ (5)	++ (3) and +++ (2)	↓
5	++ (4) and 0 (1)	+ (4) and ++ (1)	↓

Myotonic runs were measured 5 times in each *HSA^{LR}* mouse before and after treatment with TDZD-8, and the severity of myotonia is expressed from + to +++, where + corresponds to weak myotonia and +++ corresponds to severe myotonia.

show that muscle in the 1-month-old *HSA^{LR}* mice was characterized by an increased number of nuclei located beneath the basal lamina and by an increased number of small-size myofibers (Figure 6). In agreement with this, the levels of marker of satellite cells Pax-7 were significantly increased in skeletal muscle of 1-month-old *HSA^{LR}* mice. The number of newly activated proliferating satellite cells also increased in young *HSA^{LR}* mice. These data suggest that in young *HSA^{LR}* mice, muscle is actively regenerating due to activation and proliferation of satellite cells. As a result, muscle regeneration prevents the development of muscle weakness. However, muscles in adult (6-month-old) *HSA^{LR}* mice had a reduced number of nuclei located beneath the basal lamina, reduced numbers of Pax-7–positive satellite cells, and reduced numbers of myofibers. These data suggest that muscle in adult *HSA^{LR}* mice cannot efficiently regenerate, and, as a result, myofibers are degenerating.

Since lithium has other targets in addition to GSK3β, we used a highly selective inhibitor of GSK3β, TDZD-8. Similar to lithium, TDZD-8 reduced muscle weakness in *HSA^{LR}* mice. This improvement in muscle strength was accompanied by a correction of GSK3β and cyclin D3 levels. The treatment of mice with TDZD-8 was more efficient than that with lithium. We observed an improvement in muscle strength in *HSA^{LR}* mice treated with lithium 2 weeks after initiation of treatment. However, the beneficial effect of TDZD-8 on muscle strength in these mice was observed within only 2 days after initiation of treatment.

In addition to improving skeletal muscle strength, the lithium and TDZD-8 treatments also reduced myotonia. The mechanism responsible for the correction of myotonia by the lithium and TDZD-8 remains to be investigated. It has been suggested that myotonia in DM1 is due to mis-splicing of the chloride channel (*CLCN1*) (42, 43). Since this splicing of *CLCN1* is regulated by two proteins, MBNL1 and CUGBP1, we suggest that activation of CUGBP1 by cyclin D3/CDK4 may improve not only the translational activity of CUGBP1, but also splicing activity, reducing myotonia. We cannot exclude the possibility that lithium and TDZD-8 treatments also have a positive effect on MBNL1 splicing activity; however, this possibility is unlikely, because GSK3β elevation occurs prior to buildup of CUG foci that sequester MBNL1 (Figure 5, C and D, Supplemental Figure 1, and refs. 22, 38).

One of the important questions to be answered is, What is the most appropriate timing for treatment of DM1 with GSK3β inhibitors? We found that TDZD-8 treatment of young (6 weeks old) *HSA^{LR}* mice for 1 week improved their grip strength by 10.9% (Supplemental Figure 4). We tested grip strength in the same mice at 3 months of age and found that their grip strength was 9.2% higher than in the age- and sex-matched untreated *HSA^{LR}* mice. These data suggest that the inhibition of GSK3β in *HSA^{LR}* mice at a young age, when they show an insignificant reduction in grip strength, delays development of muscle weakness at 3 months of age. Use of inducible mouse models with temporary expression of CUG repeats at a young age, with simultaneous treatment with lithium or other potent inhibitors of GSK3β such as TDZD-8, would be a good model for determining the best timing of treatment of these mice.

In conclusion, this study shows that the mutant CUG repeats elevate active GSK3β in DM1 muscle and that inhibition of GSK3β with lithium or TDZD-8 improves muscle strength and reduces myotonia in the DM1 mouse model. Results in this study and the data described in the literature suggest that CUG repeats cause the disease through several pathways: (a) elevation of active CUGBP1 due to an increase of its stability, causing mis-regulation of translation, splicing, and stability of mRNAs controlled by CUGBP1; (b) reduction of MBNL1 due to sequestration by foci, causing reduction of splicing of MBNL1-regulated mRNAs; and (c) mis-regulation of signaling in DM1 cells, in particular GSK3β signaling, which leads to elevation of the inactive form of CUGBP1 in DM1 muscle. The positive effect of lithium and TDZD-8 on skeletal muscle function in *HSA^{LR}* mice suggests that lithium or other GSK3 antagonists that correct the GSK3β/cyclin D3/CUGBP1 pathway might be candidates for DM1 therapy.

Methods

Chemicals. TDZD-8 was obtained from Sigma-Aldrich. TDZD-8 was dissolved in DMSO at 10 mg/ml and kept at –80°C until use.

Muscle biopsy samples. Muscle biopsy samples from biceps brachii of 8 patients with DM1 of both sexes, aged 42–56 years, were used. Four control samples from patients with normal muscle histology were derived from 2 males and 2 females of 46, 52, 53, and 54 years of age. Muscle biopsies were kept frozen at –80°C until use.

Animals. Homozygous *HSA^{LR}* mice were a gift from Charles A. Thornton of the University of Rochester Medical Center, Rochester, New York, USA. Skeletal muscle histology of several muscle groups of *HSA^{LR}* mice of different age (1, 3, 6, and 9 months) and the age- and sex-matched WT mice was examined by H&E staining. To quantify the number of fibers, the myofibers (200–300 fibers) in the maximal cross-sectional area were counted using MetaMorph (Molecular Devices) software. Nuclei were counted in 200–300 fibers of each muscle group in maximal cross-sectional areas in the sex- and age-matched mouse cohorts using MetaMorph software, and the results were averaged. The average area of myofibers was calculated using MetaMorph software based on the analysis of 200–300 fibers in maximal cross-sectional areas of each muscle group. The grip strength in *HSA^{LR}* and matching WT mice was examined using a grip strength meter (Columbus Instruments). Measurement of grip strength in mice of different ages was performed in comparable environments. Prior the grip strength test, mice were acclimated by grasping the wire from the grip strength meter several times. During this test, the mouse was allowed to establish a firm grip on the wire, and then the mouse was slowly pulled away until the grip was released. The tension of the wire was recorded, and the average grip strength was determined based on 5 grasps for each mouse. The measurements were repeated 5 times with 5 grasps each time, and average grip strength was calculated. In the experiments with lithium

treatment, mice of 3 months of age showing muscle weakness were maintained for 2 weeks on the basic 2016 rodent diet supplemented with 0.24% lithium carbonate (Teklad, Harlan). In the experiments with TDZD-8 treatment, TDZD-8 was administered in 3-month-old HSA^{LR} mice via i.p. injections at a dose of 10 mg/kg for 2 days. Skeletal muscle strength in HSA^{LR} mice was determined before and after treatment with lithium or TDZD-8. Since TDZD-8 was dissolved in DMSO, matching HSA^{LR} mice were injected with the same amounts of DMSO as control. For biochemical analyses where indicated, soleus, gastroc, and TA from HSA^{LR} mice were collected, cut in pieces, and subjected to immediate freezing in liquid nitrogen. As a control, corresponding muscles were collected from the sex- and age-matched WT mice. Frozen muscle samples were kept at –80°C until use. In experiments with myotonia, HSA^{LR} mice showing muscle weakness were treated with lithium or TDZD-8, and myotonia was measured in the proximal rear leg muscle with monopolar electrodes before and after treatment in the EMG laboratory (Baylor College of Medicine). Each measurement was repeated 5 times at the same temperature (32°C), and myotonic runs were recorded. No sedation was applied. The severity of myotonia was estimated from + to +++, with + corresponding to weak myotonia and +++ corresponding to severe myotonia.

Analysis of activated satellite cells. To isolate activated satellite cells, whole muscle (gastroc) from sex- and age-matched WT (n = 5), HSA^{LR} (n = 4), and HSA^{LR} mice treated with TDZD-8 (n = 2) were minced and digested in a solution of 0.5% collagenase II (Gibco, Invitrogen) in 1× PBS for 45 minutes at 37°C with gentle agitation. The digested muscle was filtered through Netwell inserts with mesh size polyester membrane, and supernatants were plated in 2-chamber slides in HAM's F-10 medium, containing 15% FBS, 5% defined supplemented calf serum, 2 mmol/l L-glutamine, 100 μg/ml penicillin/streptomycin, and 0.5 μg/ml human basic fibroblast growth factor. Cells maintained for 17 hours in 5% CO_2 at 37°C were washed in 1× PBS and fixed in 4% formaldehyde. Satellite cells were identified by immunofluorescence analysis with polyclonal antibodies to Pax-7 (no. ab34360) from Abcam. Fixed cells were sequentially incubated in a solution of 1× PBS, containing normal goat serum (1:25) and 0.5% BSA, then with primary antibodies to Pax-7 (diluted 1:150 in 1× PBS, supplemented with normal goat serum,1:200, and 0.2% BSA), and with secondary goat anti-rabbit antibodies labeled with FITC (1:200, Santa Cruz Biotechnology Inc.). Slides were mounted in Vectashield medium (Vector Laboratories) containing DAPI. Pax-7–positive cells were visualized by fluorescence microscopy as shown in Supplemental Figures 2 and 3. As a control for the immunofluorescence study, the primary antibodies were omitted (Supplemental Figure 2A). For comparison of the number of satellite cells in the matching WT, HSA^{LR}, and HSA^{LR} mice treated with TDZD-8, each slide chamber was divided into 40 sections, and all Pax-7–positive cells were counted under the same conditions (magnification, time of exposure, contrast, and brightness) using MetaMorph software. The average values of 3 experiments were obtained and normalized to the weight of the whole gastroc in the analyzed mice.

Western blot assay. Normal and DM1 myoblasts were grown as previously described (15, 21). Myotube differentiation was initiated by the switching of the growth medium containing FBS to the fusion medium lacking FBS (15, 21). The efficiency of myotube differentiation was monitored by light microscopy and by Western blot analysis with antibodies against protein markers of differentiation. Cytoplasmic and nuclear protein extracts were isolated from cultured cells as described previously (7, 8). The efficiency of the separation of cytoplasm and nucleus was examined by Western blot assay with antibodies to Rb (nuclear protein) and to HSP70 (preferentially cytoplasmic protein). Frozen human and mouse muscle samples were homogenized in RIPA buffer containing pepstatin (0.7 μg/ml), leupeptin (0.5 μg/ml), and a cocktail of inhibitors of phosphatases (Sigma-Aldrich) (1 μg/ml) using an electric homogenizer. Protein extracts were centrifuged at 2.4 *g* for 10 minutes at 4°C. Supernatants were collected and frozen in portions at –80°C. Proteins (50 μg) were separated by SDS–gel electrophoresis, transferred onto nitrocellulose, and probed with monoclonal antibodies to CUGBP1 (no. sc-56649), cyclin D3 (no. sc-182), total GSK3β (no. sc-71186), p-S9–GSK3β (no. sc-11757), p-Y216–GSK3β (no. sc-135653), total GSK3α (no. sc-5264), Pax-7 (no. sc-81975) (all from Santa Cruz Biotechnology Inc.), p-T283–cyclin D1 (no. ab55322) from Abcam, and β-actin (no. A5441) from Sigma-Aldrich.

Immunoprecipitation–Western blot assay. Total cyclin D3 was precipitated with antibodies to cyclin D3 (sc-18, Santa Cruz Biotechnology Inc.) from protein extracts isolated with RIPA buffer. Since cyclin D3 is reduced in DM1 muscle, the amount of DM1 muscle tissue used for the IP was 600 mg, whereas the amount of normal muscle tissue used was 100 mg. The cyclin D3 IPs were divided into two portions. One portion was used for Western blot analyses with antibodies to p-T283–cyclin D1 and to total cyclin D3. The second portion of the cyclin D3 IP was examined by Western blot antibodies to Rb. The experiments were repeated 3 times, and average values were presented.

*Stability of GSK3*β. Normal and DM1 myoblasts (grown no more than 12 passages) were maintained at 50% density as described previously (15). CHX (final concentration, 10 mM) was added to the growth medium, and cytoplasmic and nuclear proteins were collected at 0, 1, 2, and 4 hours after CHX addition. Proteins were analyzed by Western blot assay with antibodies to total GSK3β and β-actin as control for loading.

*Treatment of GSK3*β *with lithium in Tet-regulated* CUG_{914} *CHO monoclonal cell lines*. The generation, conditions of growth, and characterization of the Tet-on CHO cell line expressing noncoding RNA containing 914 pure CUG repeats and GFP from the two independent CMV promoters have been described previously (22, 38). Briefly, the CHO monoclonal cell line (clone 2) was grown to 70% density in DMEM containing 10% Tc-free FBS and antibiotics, Geneticin (250 μg/ml) and Hygromycin B (400 μg/ml). In parallel plates, LiCl (20 μM) was added. Transcription of CUG_{914} was induced by addition of Dox (350 ng/ml); RNA and protein extracts were collected at different time points after Dox addition (0, 7, 17, 24, and 48 hours). Expression of CUG_{914} RNA in this cell culture model, examined by Northern blot hybridization with ^{32}P-labeled CAG_7 probe, was previously reported (22, 38). Expression of GFP after Dox addition was examined by monitoring of fluorescent signal. Proteins were extracted from nuclei and cytoplasm as described previously (7, 8) and used for Western blot analysis (50 μg) with antibodies to total GSK3β, cyclin D3, and β-actin as a control for loading. The accumulation of CUG foci in CHO monoclonal cells expressing CUG_{914} RNA was examined by FISH hybridization with CAG_{15} probe, labeled with Alexa Fluor 555, as described previously (38).

Statistical analyses and densitometric analysis. Western blot and IP–Western blot images were quantified by scanning densitometry using 3 measurements. The values were normalized to actin expression levels. Mean values (based on 3 independent experiments) were presented as fold change relative to controls. For statistical analysis of the grip strength in mice of different ages, 2-way ANOVA and 2-tailed Student's t test were used. Statistical analysis of total fiber number, myofiber area, and number of internal and external nuclei in 2 muscle groups of mice of 2 genotypes and of different ages was performed using 3-way ANOVA and 2-tailed Student's t test. For statistical analysis of grip strength in mice treated with lithium and TDZD-8, 2-tailed Student's t test was used. A P value less than 0.05 was considered statistically significant.

Study approval. A protocol dealing with animal use was approved by the Institutional Animal Care and Use Committee at Baylor College of Medicine. All animal work was performed in accordance with the NIH

Guide for the Care and Use of Laboratory Animals (NIH publication no. 85-23. Revised 1985). The use of human muscle samples was conducted according to the Human Subject Protocol, approved by the Institutional Review Board, Baylor College of Medicine. Patients provided written informed consent.

Acknowledgments

The authors are thankful to rotation student John Leach for the initial experiments with mouse treatment. This work was supported by NIH grants 2R01-AR044387-13, 2R01-AR052791-07, R21-NS078659 (to L.T. Timchenko), 2T32HL007676-21A1 (to K. Jones), GM551888, CA100070, AG039885, AG028865, and CA159942 (to N.A. Timchenko) and a grant from Association Française Contre les Myopathies (to G. Meola).

Received for publication April 5, 2012, and accepted in revised form September 21, 2012.

Address correspondence to: Lubov Timchenko, Department of Molecular Physiology and Biophysics, Baylor College of Medicine, One Baylor Plaza, Houston, Texas 77030, USA. Phone: 713.798.6911; Fax: 713.798.3142; E-mail: lubovt@bcm.edu.

1. Harper PS. *Myotonic Dystrophy*. London, United Kingdom: WB Saunders; 2001.
2. Brook JD, et al. Molecular basis of myotonic dystrophy: expansion of a trinucleotide (CTG) repeats at the 3′ end of a transcript encoding a protein kinase family member. *Cell.* 1992;68(4):799–808.
3. Fu YH, et al. An unstable triplet repeat in a gene related to myotonic muscular dystrophy. *Science*. 1992; 255(5049):1256–1258.
4. Reardon W, Newcombe R, Fenton I, Sibert J, Harper PS. The natural history of congenital myotonic dystrophy: mortality and long term clinical aspects. *Arch Dis Child.* 1993;68(2):177–181.
5. Amack JD, Mahadevan MS. Myogenic defects in myotonic dystrophy. *Dev Biol.* 2004;265(2):294–301.
6. Wang J, et al. Myotonic dystrophy: evidence for a possible dominant-negative RNA mutation. *Hum Mol Genet.* 1995;4(4):599–606.
7. Timchenko LT, Timchenko NA, Caskey CT, Roberts R. Novel proteins with binding specificity to DNA CTG and RNA CUG repeats: implications for myotonic dystrophy. *Hum Mol Genet*. 1996; 5(1):115–121.
8. Timchenko LT, et al. Identification of a (CUG)n triplet repeat binding protein and its expression in myotonic dystrophy. *Nucleic Acids Res.* 1996; 24(22):4407–4414.
9. Philips AV, Timchenko LT, Cooper TA. Disruption of splicing of regulated by CUG binding protein in myotonic dystrophy. *Science.* 1998;280(5364):737–741.
10. Timchenko LT. Myotonic dystrophy: the role of RNA CUG repeats. *Am J Hum Genet*. 1999; 64(2):360–364.
11. Mankodi A, et al. Myotonic dystrophy in transgenic mice expressing an expanded CUG repeat. *Science.* 2000;289(5485):1769–1772.
12. Miller JW, et al. Recruitment of human muscleblind proteins to (CUG)n expansions associated with myotonic dystrophy. *EMBO J.* 2000;19(17):4439–4448.
13. Seznec H, et al. Mice transgenic for the human myotonic dystrophy with expanded CTG repeats display muscular and brain abnormalities. *Hum Mol Genet.* 2002;10(23):2717–2726.
14. Timchenko NA, Cai ZJ, Welm AL, Reddy S, Ashizawa T, Timchenko LT. RNA CUG repeats sequester and alter protein levels and activity of CUGBP1. *J Biol Chem*. 2001;276(11):7820–7826.
15. Timchenko NA, Iakova P, Cai ZJ, Smith JR, Timchenko LT. Molecular basis for impaired muscle differentiation in myotonic dystrophy. *Mol Cell Biol.* 2001;21(20):6927–6938.
16. Savkur RS, Philips AV, Cooper TA. Aberrant regulation of insulin receptor alternative splicing is associated with insulin resistance in myotonic dystrophy. *Nat Genet*. 2001;29(1):40–47.
17. Kanadia RN, et al. A muscleblind knockout model for myotonic dystrophy. *Science.* 2003; 302(5652):1978–1980.
18. Timchenko NA, Patel R, Iakova P, Cai ZJ, Quan L, Timchenko LT. Overexpression of CUG triplet repeat-binding protein, CUGBP1, in mice inhibits myogenesis. *J Biol Chem.* 2004;279(13):13129–13139.
19. Mahadevan MS, et al. Reversible model of RNA toxicity and cardiac conduction defects in myotonic dystrophy. *Nat Genet.* 2006;38(9):1066–1070.
20. Orengo JP, Chambon P, Metzger D, Mosier DR, Snipes GJ, Cooper TA. Expanded CTG repeats within the DMPK 3′ UTR causes severe skeletal muscle wasting in an inducible mouse model for myotonic dystrophy. *Proc Natl Acad Sci U S A.* 2008; 105(7):2646–2651.
21. Salisbury E, et al. Ectopic expression of cyclin D3 corrects differentiation of DM1 myoblasts through activation of RNA CUG-binding protein, CUGBP1. *Exp Cell Res.* 2008;314(11–12):2266–2278.
22. Huichalaf C, et al. Expansion of CUG RNA repeats causes stress and inhibition of translation in myotonic dystrophy 1 (DM1) cells. *FASEB J.* 2010; 24(10):3706–3719.
23. Ebralidze A, Wang Y, Petkova V, Ebralidse K, Junghans RP. RNA leaching of transcription factors disrupts transcription in myotonic dystrophy. *Science.* 2004;303(5656):383–387.
24. Kuyumcu-Martinez NM, Wang GS, Cooper TA. Increased steady-state levels of CUGBP1 in myotonic dystrophy are due to PKC-mediated hyperphosphorylation. *Mol Cell.* 2007;28(1):68–78.
25. Timchenko NA, Welm AL, Lu X, Timchenko LT. CUG repeat binding protein (CUGBP1) interacts with the 5′ region of C/EBP beta mRNA and regulates translation of C/EBPbeta isoforms. *Nucleic Acids Res.* 1999;27(22):4517–4525.
26. Paillard L, Omilli F, Legagneux V, Bassez T, Maniey D, Osborne HB. EDEN and EDEN-BP, a cis element and an associated factor that mediate sequence-specific mRNA deadenylation in Xenopus embryos. *EMBO J.* 1998;17(1):278–287.
27. Webster PJ, Liang L, Berg CA, Lasko P, Macdonald PM. Translational repressor bruno plays multiple roles in development and is widely conserved. *Genes Dev*. 2007;11(19):2510–2521.
28. Moraes KC, Wilusz CJ, Wilusz J. CUG-BP binds to RNA substrates and recruits PARN deadenylase. *RNA.* 2006;12(6):1084–1091.
29. Timchenko NA, Wang GL, Timchenko LT. RNA CUG-binding protein 1 increases translation of 20-kDa isoform of CCAAT/Enhancer-binding protein beta by interacting with the alpha and beta subunits of eukaryotic initiation translation factor 2. *J Biol Chem*. 2005;280(21):20549–20557.
30. Lee JE, Lee JY, Wilusz J, Tian B, Wilusz CJ. Systematic analysis of cis-elements in unstable mRNAs demonstrates that CUGBP1 is a key regulator of mRNA decay in muscle cells. *PLoS One.* 2010;5(6):e11201.
31. Rattenbacher B, et al. Analysis of CUGBP1 targets identifies GU-repeat sequences that mediate rapid mRNA decay. *Mol Cell Biol.* 2010;30(16):3970–3980.
32. Timchenko LT, et al. Age-specific CUGBP1-eIF2 complex increases translation of CCAAT/Enhancer-binding protein beta in old liver. *J Biol Chem*. 2006; 281(43):32806–32819.
33. Naderi S, et al. cAMP-induced degradation of cyclin D3 through association with GSK-3β. *J Cell Sci.* 2004; 117(pt 17):3769–3783.
34. De Santa F, Albini S, Mezzaroma E, Baron L, Felsani A, Caruso M. pRb-dependent cyclin D3 protein stabilization is required for myogenic differentiation. *Mol Cell Biol*. 2007;27(20):7248–7265.
35. Doble BW, Woodgett JR. GSK-3: tricks of the trade for a multi-tasking kinase. *J Cell Sci.* 2003; 116(pt 7):1175–1186.
36. Jin J, Wang GL, Shi X, Darlington GJ, Timchenko NA. The age-associated decline of glycogen synthase kinase 3β plays a critical role in the inhibition of liver regeneration. *Mol Cell Biol.* 2009; 29(14):3867–3880.
37. Cole A, Frame S, Cohen P. Further evidence that the tyrosine of glycogen synthase kinase-3 (GSK3) in mammalian cells is an autophosphorylation event. *Biochem J.* 2004;377(pt 1):249–255.
38. Jones K, et al. RNA foci, CUGBP1, and ZNF9 are the primary targets of the mutant CUG and CCUG repeats expanded in myotonic dystrophies type 1 and type 2. *Am J Pathol.* 2011;179(5):2475–2489.
39. Morales F, et al. Somatic instability of the expanded CTG triplet repeat in myotonic dystrophy type 1 is a heritable quantitative trait and modifier of disease severity. *Hum Mol Genet.* 2012;21(16):3558–3567.
40. van Eyk CL, et al. Perturbation of the Akt/Gsk3-β signaling pathway is common to Drosophila expressing expanded untranslated CAG, CUG, and AUUCU repeat RNAs. *Hum Mol Genet*. 2011; 20(14):2783–2794.
41. Zu T, et al. Not-ATG-initiated translation directed by microsatellite. *Proc Natl Acad Sci U S A*. 2011; 108(1):260–265.
42. Charlet-B N, Savkur RS, Singh G, Philips AV, Grice EA, Cooper TA. Loss of the muscle-specific chloride ion channel in type 1 myotonic dystrophy due to misregulated alternative splicing. *Mol Cell*. 2002; 10(1):45–53.
43. Mankodi A, et al. Expanded CUG repeats trigger aberrant splicing of ClC-1 chloride channel pre-mRNA and hyperexcitability of skeletal muscle in myotonic dystrophy. *Mol Cell*. 2002;10(1):35–44.